Numerical Analysis of Triple – Barrier GaAs/ $Al_xGa_{1-x}As$ Resonant Tunneling Structure Using PMM Approach

Abbas Zarifkar, Abolfazl Mohammadi Bagherabadi

Iran Telecommunication Research Center, Tehran, Iran
Islamic Azad University, Science and Research Branch, Tehran, Iran

Summary
A theoretical study of triple barrier resonant tunneling diode with multilayer GaAs/$Al_xGa_{1-x}As$ heterostructure is presented based on an exact solution of the Schrodinger equation under the application of a constant electric field and a uniform magnetic field. Using propagation matrix method (PMM), the transmissivity of the structure is calculated as a function of the incident electron energy for different values of applied voltage. The results show good agreement with other existing models.

Key words:
Tunneling, Schrodinger Equation, PMM, RTD, Simulation, Heterostructure, GaAs/AlxGa1-xAs.

1. Introduction

Advanced crystal growth techniques, such as metal-organic vapor phase epitaxy (MOVPE) and molecular beam epitaxy (MBE) make it possible to obtain quantum wells and superlattices with reproducible properties at the atomic scale [1]. Additionally, use of in situ growth monitoring techniques such as reflection high-energy electron diffraction (RHEED) in a MBE system provides exacting control of layer thicknesses to within one monolayer. This exacting growth control enables the realization of structures with quantum-sized dimensions [2]. By using these techniques many different devices have been designed and fabricated such as resonant interband tunneling diode (RITD) resonant-tunneling diode (RTD) and resonant tunneling transistor (RTT) can have multiple on and off states associated with multiple discrete quantum levels inside the potential well on a very small or very narrow island. If these levels are spaced widely enough in energy (that is, if is greater than the energetic difference between the band edge and the Fermi level for the source), then each of the different levels in the well can be brought successively into and out of resonance with the source conduction band in succession, as the bias voltage (or gate voltage) is increased [3, 4]. The RTD, and its several variations, has become a research focus in nanoelectronics for its promise as a primary nanoelectronic device for both analog and digital applications [5]. Among the numerous nanoelectronic devices proposed and demonstrated, the RTD is perhaps the most promising candidate for digital circuit applications due to its negative differential resistance (NDR) characteristic, structural simplicity, relative ease of fabrication, inherent high speed, flexible design freedom, and versatile circuit functionality [5]. Some digital applications are Tri-State Logic [3], digital logic [6], memory cells1 and ultrafast analog digital converters [7], Logic and memory applications[8] Flip Flop ICs [9]. There are different ways to simulate RTDs. Propagation Matrix Method (PMM) is one of the most popular methods for simulation of heterostructures.

The rest of the paper is organized as follows: In Sec. 2, we present modeling of the device. In Sec. 3, based on the model in Sec. 2, simulation method is presented and the results are obtained. Finally, we conclude this paper in Sec. 4.

2. Device Modeling

In this part we describe the geometry and formulation of the device.

2.1 Geometry and Composition For The Device

The conduction-band energy diagram for a TBRT structure is shown in Fig.1. The structure consist of two heavily doped n+ GaAs layers, undoped AlGaAs barriers and the undoped GaAs quantum well (QW) regions.
For GaAs, meff1=0.067m0 and Eg1=1.424ev. For the AlxGa1-xAs, meff2=0.1168m0 Eg2= 1.424+1.247x and for x=0.373,Eg2=3.313. Thus for this structure ΔEc=0.4655ev.

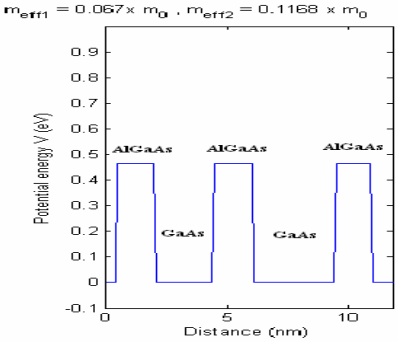

Fig.1 The conduction band diagram of the triple barrier resonant tunneling diode.

Manuscript received June 5, 2008.
Manuscript revised June 20, 2008.

2.2 Theory and Formulation

We assume for our resonant structures that the incoherent electron scattering, space-charge effects, many-electron effects and phonon-assisted tunneling are neglected. Using the effective-mass single electron approximation, we then separate the three-dimensional single-electron Schrodinger equation into parts which are transverse and parallel to the device layers. The total electron energy Etot is then written as the sum of these parallel and transverse components:

$$E_{tot} = \frac{E + \hbar^2 |k_{II}|^2}{2m^*} \quad (1)$$

where kII is the wave vector in the x-y plane parallel to the AlxGa1-xAs/GaAs interfaces. E is the electron kinetic energy perpendicular to the interfaces. The total wave function can be expressed as a product:

$$\Psi(x, y, z) = \frac{1}{\sqrt{A}} e^{ik_{II} r_{II}} \varphi(z) \quad (2)$$

A represents the device area k*II* and r*II* are vectors in the x-y direction, and j is the solution to the following one-dimensional Schrodinger equation:

$$-\frac{\hbar^2}{2}\frac{d}{dz}\left(\frac{1}{m^*(z)}\right)\frac{d\varphi}{dz} + U(z)\varphi = E\varphi \quad (3)$$

where m*(z) denotes the position-dependent electron (band gap) effective mass and U (z) is the potential seen by a single electron, which includes effects of both conduction-band discontinuities at AlxGa1-xAs /GaAs interfaces and external applied voltage.

To solve for the transmission probability, we use propagation – matrix method. This method, in which the exact potential is approximated by a series of steps, has among its advantages computational simplicity and good accuracy. The main problem is quit simple, if we treat the potential as constant over each step. In this case the solution to the one-dimensional Schrodinger equation is given in the jth step as a superposition of plane waves:

$$\varphi_j(z_j) = A_j e^{k_j z_j} + B_j e^{-k_j z_j} \quad (4)$$

and we have the z component of the complex wave vector Kj given by:

$$K_j = \left[\frac{2m_j^*(U_j - E)}{\hbar^2}\right]^{1/2} \quad (5)$$

And j=0, 1, 2, …, N, N+1 for a total of N+1 steps. Here Uj and m*j are the potential and effective mass associated with step j, and zj is distance measured from the left-hand side of the jth step. Furthermore, the steps are all assumed to have the same length *a* and *j* values increase as the structure is traversed from left to right.

Imposing continuity of the wave function j and its appropriately normalized derivative (*1/m**) (*dj /dz*) at the boundary between steps *j* and *j+1*, one derives a matrix formula:

$$\begin{bmatrix} A \\ B \end{bmatrix} = \left(\prod_{J=1}^{j=N} P_j\right)\begin{bmatrix} C \\ D \end{bmatrix} = P\begin{bmatrix} C \\ D \end{bmatrix} \quad (6)$$

where A and C are coefficients for the wave function traveling left-to-right in regions j and j+1, respectively, and B and D are the corresponding right-to-left traveling-wave coefficients [1,10]. Solving the problem with the PMM has a six steps algorithm [10].

3 Simulation Results

Because of the dependence of the device on the bias voltage we have done the simulation for different values of the bias voltage.

3.1 Simulation Results For Vbias < 0

Fig.2 implies that for negative Vbias with large absolute value the transmission coefficient is very small and increases for larger energies; and as we can see there is no tunneling region. Thus the current flow will be small for this case.

Fig.3 shows that for negative Vbias, increasing the Vbias, results in the increase in the Transmission Coefficient. Furthermore tunneling regions are appearing but these tunneling regions are not acceptable yet. We can also see that the Transmission Coefficient value is so small and we can't see unity or near unity Transmission Coefficient in the diagram which means that the current flow will be small for this case.

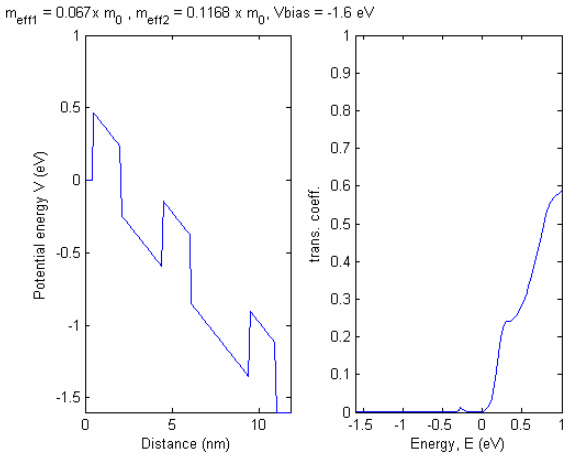

Fig.2. Potential Energy and Transmission Coefficient diagrams for the device under negative bias voltage (Vbias = - 1.6)

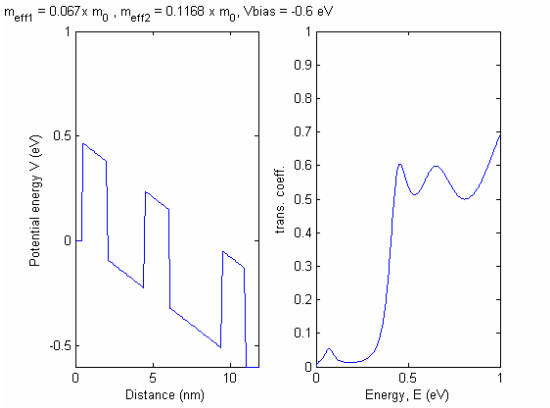

Fig.3 Potential Energy and Transmission Coefficient diagrams for the device under negative bias voltage (Vbias =- 0.6).

Fig.4 represents that for negative Vbias, near zero, the Transmission Coefficient increases. Furthermore tunneling regions are increasing. We can also see that the Transmission Coefficient value has increased but there is no unity Transmission Coefficient in the diagram.

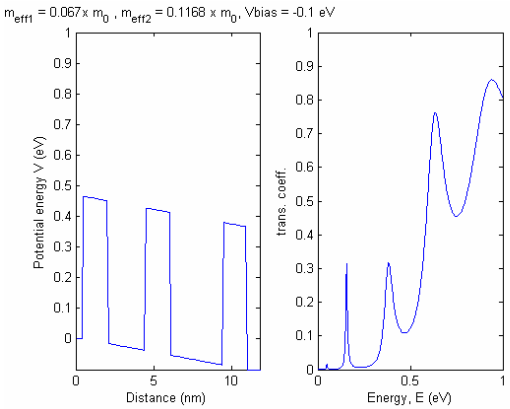

Fig.4 Potential Energy and Transmission Coefficient diagrams for the device under negative bias voltage (Vbias= - 0.1).

3.2 Simulation Results For Vbias = 0

Fig.5 represents that for Vbias=0, the Transmission Coefficient increases. Furthermore tunneling regions are increasing. We can also see that the Transmission Coefficient value has increased but there is no unity Transmission Coefficient in the diagram.

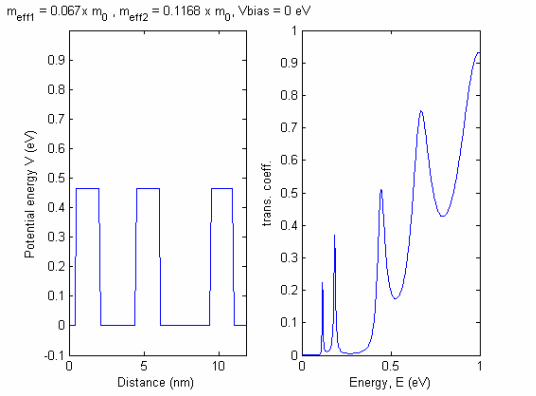

Fig.5 Potential Energy and Transmission Coefficient diagrams for the device under no bias voltage (Vbias =0).

3.3 Simulation Results For Vbias > 0

Fig.6 represents that for a small value of Vbias (0.1), the Transmission Coefficient increases. Furthermore the Transmission Coefficient value has increased and there is a unity peak Transmission Coefficient in the diagram for the energy near Vbias. This peak exists because an electron incident from the left tunnels via the resonance in the potential well at this energy.

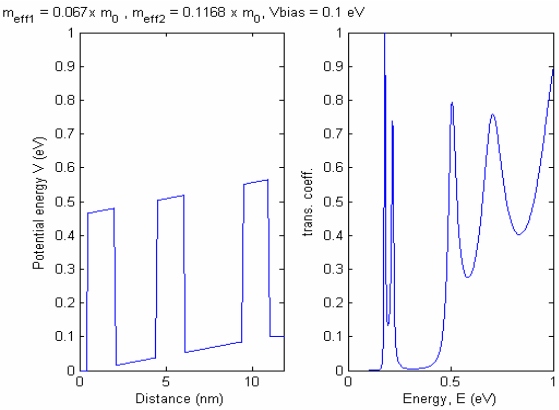

Fig.6 Potential Energy and Transmission Coefficient diagrams for the device under positive bias voltage (Vbias = 0.1).

Fig.7 shows that for a larger value of Vbias (0.3), the Transmission Coefficient increases. Furthermore the Transmission Coefficient value has increased and there are two unity peaks in the Transmission Coefficient diagram for the energy near Vbias. The first peak exist because an electron incident from the left tunnels via the resonance in the potential well at the energy equal to Vbias, and the second is because of resonance tunneling in the device

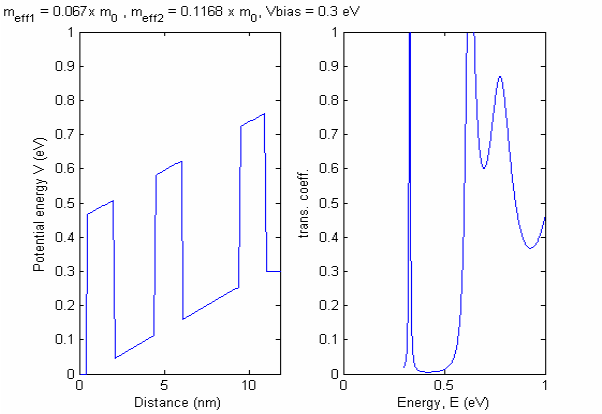

Fig.7 Potential Energy and Transmission Coefficient diagrams for the device under positive bias voltage (Vbias = 0.3).

Fig.8 implies that for Vbias equal to the barrier energy the Transmission Coefficient value has increased and there are two peaks in the Transmission Coefficient diagram for the energy near Vbias. The peaks and the negative slope represent the tunneling via the resonance in the potential wells and the negative resistance property of the device.

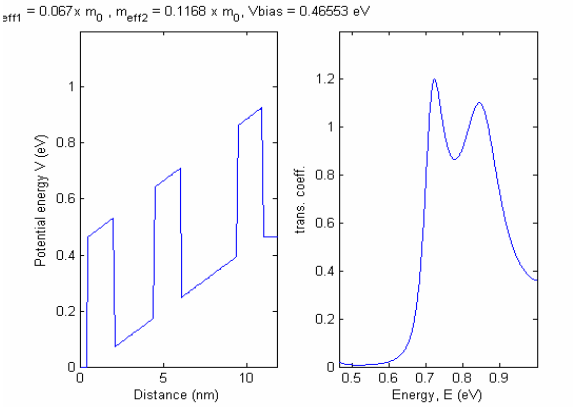

Fig.8 Potential Energy and Transmission Coefficient diagrams for the device under positive bias voltage (Vbias = 0.46553).

Fig.9 represents that for Vbias much more larger than the barrier potential the transmission coefficient increases fore larger energies and as we can see there is only one peak more then unity in the diagram means that the transmission due to tunneling has decreased and this is obvious because the energy of most of the particles is much more than the energy of the barriers.

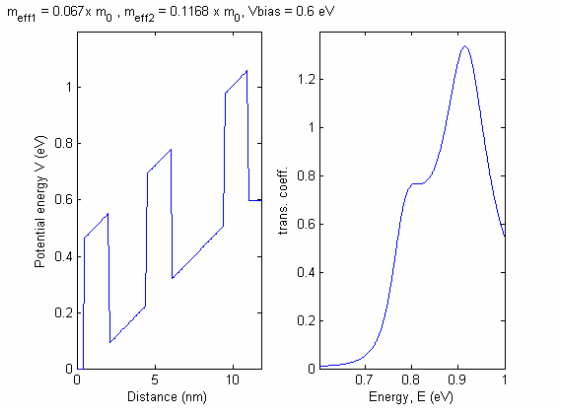

Fig.9 Potential Energy and Transmission Coefficient diagrams for the device under positive bias voltage (Vbias = 0.6).

4 Conclusion

In this paper we have numerically examined the transmission coefficient in GaAs/ AlxGa1-xAs triple-barrier structures. We examined our structure for different biases and concluded that for negative values of bias voltage there is no unity transmission coefficient but we can observe tunneling phenomena. Increasing the bias voltage results in the increase of the transmission coefficient peaks but for negative values of bias voltage there is no unity peak in the transmission coefficient means that no resonance tunneling occurs. For positive values of bias voltage we can observe resonant tunneling because of one or more unity transmission coefficient. For bias voltages much more larger than the barrier potential the transmission coefficient increases fore larger energies and as we can see there is only one peak more than unity in the

diagram which means that the transmission due to tunneling has decreased and this is obvious because the energy of most of the particles is much more than the energy of the barriers.

References

[1] C. E. Simion, and C. I. Ciucu "Triple barrier resonant tunneling : A transfer matrix approach" Romanian Reports in Physics, vol. 59, Number 3, pp. 803-814, Sept. 2007.

[2] K. F. Brennan, and A.S. Brown, Theory of Modern Electronic Semiconductor Devices. John Wiley and Sons, Inc., New York, 2002.

[3] Niu Jin, , S.Y. Chung, , R.M. Heyns, P. R. Berger, , R. Yu P. E. Thompson , and S. L. Rommel, "Tri-State Logic Using Vertically Integrated Si–SiGe Resonant Interband Tunneling Diodes With Double NDR", IEEE Electron Device Lett., vol. 25, pp. 646-648, 2004.

[4] D. G. Gordon, M. S. Montemerlo, J. C. Love, G. J. Opiteck, and J.C Ellenborgen "Overview of nanoelectronic devices", Proc. of the IEEE vol. 85, pp. 521–540, 1997.

[5] J. P. Sun, G. I. Haddad, P. Mazumder, and J. N. Schulman, "Resonant Tunneling Diodes: Models and Properties", Proceedings of IEEE, vol. 86, No.4, pp.641-661, 1998.
[6] P. Mazumder, S. Kulkarni, M. Bhattacharya, J. P. Sun, and G. I. Haddad, "Digital circuit applications of resonant tunneling devices," Proc. IEEE, vol. 86, pp. 664–686, Apr. 1998.
[7] T. Sandu, G. Klimeck, and W. P. Kirk, "Off-center electron transport in resonant tunneling diodes due to incoherent scattering", Phys. Rev. B, vol. 68, pp.(115320-1) - (115320-9), 2003.
[8] S.-Y. Chung, N. Jin, R. E. Pavlovicz, R. Yu, Paul R. Berger, and P. E. Thompson, "Analysis of the Voltage Swing for Logic and Memory Applications in Si/SiGe Resonant Interband Tunnel Diodes Grown by Molecular Beam Epitaxy", IEEE Trans. on Nanotechnology, vol. 6, No. 2, March 2007.
[9] T. KIM, B. LEE, S. CHOI, and K. YANG, "Resonant Tunneling Diode/HBT D-Flip Flop ICs Using Current Mode Logic-Type Monostable-Bistable Transition Logic Element with Complementary Outputs", Japanese Journal of Applied Physics, vol. 44, No. 4B, pp. 2743–2746, 2005.
[10] A. F. J. Levi, Applied Quantum Mechanics, Cambridge University Press, Edition 2, 2006.